Effect of Four Helix Bundle Topology on Heme Binding and Redox Properties†

Brian R. Gibney, Francesc Rabanal, Konda S. Reddy, and P. Leslie Dutton*

Johnson Research Foundation, Department of Biochemistry and Biophysics, University of Pennsylvania, Philadelphia, Pennsylvania 19104

Received July 30, 1997; Revised Manuscript Received January 27, 1998

ABSTRACT: We have designed two alternative four helix bundle protein scaffold topologies for maquette construction to examine the effect of helix orientation on the heme binding and redox properties of our prototype heme protein maquette, $(\alpha\text{-SS-}\alpha)_2$, previously described as H10H24 [Robertson, D. E., Farid, R. S., Moser, C. C., Mulholland, S. E., Pidikiti, R., Lear, J. D., Wand, A. J., DeGrado, W. F., and Dutton, P. L. (1994) *Nature 368,* 425]. Conversion of the disulfide-bridged di-α-helical monomer of $(\alpha\text{-SS-}\alpha)_2$ into a single polypeptide chain results in topological reorientation of the helix dipoles and side chains within a 62 amino acid helix-loop-helix monomer, (α-*l*-α), which self-associates to form $(\alpha\text{-}l\text{-}\alpha)_2$. Addition of an N-terminal cysteine residue to (α-*l*-α) with subsequent oxidation yields a 126 amino acid single molecule four helix bundle, (α-*l*-α-SS-α-*l*-α). Gel permeation chromatography demonstrated that $(\alpha\text{-SS-}\alpha)_2$ and $(\alpha'\text{-SS-}\alpha')_2$, a uniquely structured variant of the prototype, as well as $(\alpha\text{-}l\text{-}\alpha)_2$ and $(\alpha'\text{-}l\text{-}\alpha')_2$ assemble into distinct four helix bundles as designed, whereas (α-*l*-α-SS-α-*l*-α) elutes as a monomeric four α-helix bundle. Circular dichroism (CD) spectroscopy proves that these peptides are highly α-helical, and incorporation of four hemes has little effect on the helical content of the secondary structure. Four heme dissociation constants were evaluated by UV−visible spectroscopy and ranged from the 15 nM to 25 μM range for each of the peptides. The presence of Cotton effects in the visible CD illustrated that the hemes reside within the protein architecture. The equilibrium redox midpoint potentials (E_{m8}) of the four bound hemes in each peptide are between −100 and −280 mV, as determined by redox potentiometry. The heme affinity and spectroelectrochemical properties of the hemes bound to $(\alpha\text{-}l\text{-}\alpha)_2$ and (α-*l*-α-SS-α-*l*-α) are similar to those of the prototype, $(\alpha\text{-SS-}\alpha)_2$, and to bis-histidine ligated *b*-type cytochromes, regardless of the global architectural changes imposed by these topological rearrangements. The hydrophobic cores of these peptides support local electrostatic fields which result in nativelike heme chromophore properties (spectroscopy, elevated reduction potentials, heme−heme charge interaction, and reactivity with exogenous diatomics) illustrating the utility of these non-native peptides in the study of metalloproteins.

Hemoproteins serve numerous and diverse functions within biological systems (*1*). Moreover, a single prosthetic group, [Fe(II/III)(protoporphyrin IX)], is found to be active in proteins by promoting reversible dioxygen binding (in hemoglobin and myoglobin) (*2*), electron transport (in cytochromes) (*3*), catalysis of hydrogen peroxide disproportionation (in catalases) (*4*), organic substrate oxidation (in mono and dioxygenases) (*5*), reduction of dioxygen to water (in terminal oxidases) (*6*), and gene regulation (*7*). Heme reactivity is well acknowledged to be controlled in these natural systems by selected iron ligand motifs, spin states and coordination numbers with added environmental modulation by specific interactions with amino acids, the local dielectric strength, electric fields (*8*), hydrophobicity, and water solvent exposure. However, many of the molecular descriptions of these interactions remain to be determined.

We are studying the foundations of heme−protein interactions in complex natural redox enzymes that give rise to this range of biochemistry. The approach we are using is to design and synthesize peptides that self-assemble to incorporate prosthetic groups and cofactors thereby generating simplified functional versions of complex native enzymes, maquettes (*9*). Recent advances in protein design using the minimalist (*10*−*17,53*) and binary patterning (*18,19*) approaches to the design of tetra-α-helical bundles, a ubiquitous and functionally important architectural component in native enzymes (*20*), provide for convenient construction of stable scaffolds for maquettes. Our successes as well as those of others with the incorporation of a variety of single cofactors [hemes (*9,21*) and other metalloporphyrins (*22*), free-base porphyrin dimers (*23,24*), nitroxide spin-labels (*25*), iron sulfur clusters (*26*−*29*), flavins (*30*), mononuclear metal sites (*31*−*33*)] and their subsequent combinations ([hemes and iron sulfur clusters (*26*), hemes and flavins (*30*)] open the door to systematic investigations of the interaction of cofactors and synthetic peptides and the resulting properties of functional proteins.

The focus of the present contribution is the characterization of effects on heme−protein properties of three distinct tetra-

† This work was supported by NIH Grants GM 41048 and GM 27309 to P.L.D. This work was also part of NSF MRSEC IRG DMR96-32598. B.R.G. gratefully acknowledges receipt of a postdoctoral fellowship from the National Institutes of Health (GM 17816). F.R. was supported by a postdoctoral fellowship from the European Molecular Biology Organization.

* Author to whom correspondence should be addressed.

S0006-2960(97)01856-4 CCC: $15.00
Published on Web 03/13/1998

α-helical bundle architectures designed to transform the prototype heme protein maquette, $[H10H24]_2$ or $(\alpha\text{-SS-}\alpha)_2$, the four α-helix bundle comprised of a dimer of two disulfide-linked α-helices (α-SS-α), into a single molecule four helix bundle, (α-*l*-α-SS-α-*l*-α). The influence of altered global four helix bundle topology and helix dipole composition on the helical content, global stability, heme protein binding affinity, electrochemical properties and reactivity of the bound hemes toward an exogenous diatomic, CO, is determined.

EXPERIMENTAL PROCEDURES

Materials

Hemin [Fe(III)protoporphyrin IX chloride], diethyl ether, piperidine, trifluoroacetic acid, and ^{13}CO were obtained from Aldrich Chemical Co. (Milwaukee, WI). Natural abundance CO was obtained from BOC Gases (Murray Hill, NJ). 9-Fluorenylmethoxycarbonyl (Fmoc)[1]-protected amino acid pentafluorophenyl esters (OPfp) were purchased from PerSeptive Biosystems (Framingham, MA), except for Fmoc-L-Arg(Pmc)−OPfp, which was obtained from Bachem (King of Prussia, PA). NovaSyn PR-500 resin was purchased from Calbiochem-Novabiochem (La Jolla, CA). Ethanedithiol and hydroxybenzotriazole were purchased from Fluka (Ronkonkoma, NY). Guanidine hydrochloride (8 M) was used as received from Pierce (Rockford, IL). All other chemicals and solvents were reagent grade.

Methods

Peptide Synthesis. The peptides were synthesized at 0.2 mmol scale on a continuous flow Milligen 9050 solid-phase peptide synthesizer using standard Fmoc/^{t}Bu protection strategies (*34*) with NovaSyn PR-500 resin. The side chain protecting groups used are as follows: Cys (Trt), Lys (^{t}Boc), His (^{t}Boc), Glu (O^{t}Bu), and Arg (Pmc). Prior to cleavage from the resin, the N-terminal amine was acetylated. The individual peptides were cleaved and simultaneously deprotected using 90:8:2 trifluoroacetic acid:ethanedithiol:water for 2 h. The crude peptides were precipitated and washed with cold ether, dissolved in water containing 0.1% (v/v) trifluoroacetic acid, lyophilized to powders, and purified to homogeneity by reversed phase C_{18} HPLC using aqueous acetonitrile gradients containing 0.1% (v/v) TFA. The identity of each resulting peptide was confirmed by laser desorption mass spectrometry.

Solution Molecular Mass Determination. Analytical size exclusion chromatography was performed on a Beckman System Gold HPLC system with a diode array detector using a Pharmacia Superdex 75 column equilibrated with aqueous buffer (10 mM KP_i, 100 mM KCl, pH 8.0). A flow rate of 1.0 mL/min was utilized with detection at 220 and 411 nm for the amide and heme chromophores, respectively. The column was standardized using the globular proteins aprotinin (MW = 6.5 kDa), horse heart cytochrome *c* (MW =12.1 kDa), chymotrypsinogen (MW = 25.0 kDa), ovalbumin (MW = 43.0 kDa), and bovine serum albumin (MW = 67.0 kDa).

Circular Dichroism Spectropolarimetry. CD spectra were recorded on an AVIV 62DS spectropolarimeter using rectangular quartz cells of 1.0 and 0.2 cm path length. Thermal control was maintained by a thermoelectric unit with a Neslab CFT-33 refrigerated recirculating water bath as a heat sink. Peptide concentrations were between 5 and 15 μM as determined spectrophotometrically using $\epsilon_{280} = 5600$ M^{-1} cm^{-1} for tryptophan or $\epsilon_{412} = 120\,000$ M^{-1} cm^{-1} for oxidized heme.

Heme Incorporation. A DMSO solution of hemin, 1−3 mM, was added in 0.1 equiv aliquots to peptide solutions, 20−100 μM (10 mM KP_i, 100 mM KCl, pH 8.0), with 10 min equilibration between additions.

FPLC Purification of Holo Peptide. Preparative size exclusion chromatography was performed on a Beckman System Gold HPLC system with a diode array detector using a High Load 16/60 Superdex 75 prep grade column eluted with aqueous buffer (10 mM KP_i, 100 mM KCl, pH 8.0) at a 2 mL/min flow rate. The sample provided a chromatogram consistent with that obtained from the analytical size exclusion column. The four helix bundle fraction was collected and concentrated in Centriprep-3 centrifugal force concentrators in a Beckman J-21C centrifuge. Analytical size exclusion chromatography of the concentrated peptide displayed a single species of molecular mass consistent with a four helix bundle aggregation state.

Redox Potentiometry. Chemical redox titrations (*35*) were performed in an anaerobic cuvette equipped with a platinum working and a calomel reference electrode. Ambient redox potentials (measured against the standard hydrogen electrode) were adjusted by addition of aliquots (<1 μL) of sodium dithionite or potassium ferricyanide. Titrations were performed in 10 mM potassium phosphate, 100 mM KCl, pH 8.0. Electrode−solution mediation was facilitated by the following mediators at 10μM concentration: 2-hydroxy-1,4-naphthoquinone, anthroquinone-2-sulfonate, duroquinone, phenazine ethosulfate, phenazine methosulfate, 1,4-benzoquinone, 1,2-naphthoquinone, and 1,4-naphthoquinone. After equilibration at each potential, the optical spectrum was recorded. Reduction of the hemes was followed by the increase in the α-band absorption at 559 nm. Spectral intensity was plotted against potential, and the data were fit to four independent Nernst equations with $n = 1.0$ (fixed).

UV−Vis Spectroscopy. UV−visible spectra were recorded on a Perkin-Elmer Lambda 2 spectrophotometer using quartz cells of 0.2 and 1.0 cm path length. Peptide concentrations were between 3 and 5 μM as determined spectrophotometrically using $\epsilon_{412} = 120\,000$ M^{-1} cm^{-1} for oxidized heme or $\epsilon_{280} = 5600$ M^{-1} cm^{-1} for tryptophan.

Denaturation Studies. Peptide denaturation curves of the dimeric peptides, $(\alpha\text{-SS-}\alpha)_2$, $(\alpha\text{-}l\text{-}\alpha)_2$, $(\alpha'\text{-SS-}\alpha')_2$ and $(\alpha'\text{-}l\text{-}\alpha')_2$, were fit to a dimer folded to monomer unfolded equilibrium (*36*) using a nonlinear least squares routine in KaleidaGraph (Abelbeck Software) to the following equation:

$$\text{fraction folded} = 1 - (K_{unf}/4P)[(1 + 8P/K_{unf})^{1/2} - 1]$$

[1] Abbreviations: Fmoc, 9-fluorenylmethoxycarbonyl; OPfp, pentafluorophenyl ester; Pmc, 2,2,5,7,8-pentamethylchroman-6-sulfonyl; ^{t}Boc, *tert*-butoxycarbonyl; Trt, trityl or triphenylmethyl; O^{t}Bu, *tert*-butyl ester; HOBt, 1-hydroxybenzotriazole; CD, circular dichroism; Θ_{222}, ellipticity at 222 nm; Gdn·HCl, guanidine hydrochloride; EPR, electron paramagnetic resonance; SHE, standard hydrogen electrode; HPLC, high-performance liquid chromatography; ΔG_{unf}, difference in Gibbs free energy between denatured and folded protein; DMSO, dimethyl sulfoxide; DMF, *N*,*N*-dimethylformamide.

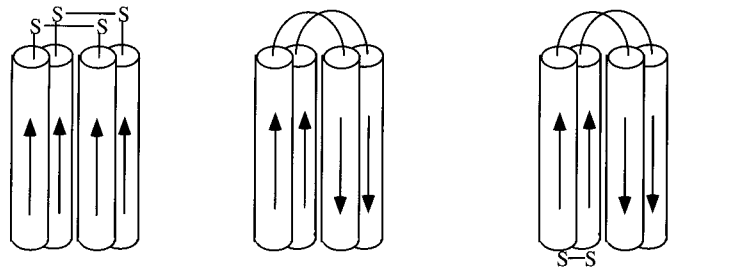

(α-SS-α) = [CGGGELWKL•HEELLKK•FEELLKL•HEERLKK•L]$_2$

(α'-SS-α') = [CGGGEIWKL•HEEFLKK•FEELLKL•HEERLKK•L]$_2$

(α-ℓ-α) = L•KKLREEH•LKLLEEF•KKLLEEH•LKWLEGGGG-
GGGGELLKL•HEELLKK•FEELLKL•HEERLKK•L

(α'-ℓ-α') = L•KKLREEH•LKLLEEF•KKLFEEH•LKWIEGGGG-
GGGGEIWKL•HEEFLKK•FEELLKL•HEERLKK•L

(α-ℓ-α-SS-α-ℓ-α) = [CL•KKLREEH•LKLLEEF•KKLLEEH•LKWLEGGGG-
GGGGELLKL•HEELLKK•FEELLKL•HEERLKK•L]$_2$

FIGURE 1: Schematic models of the three architectural frameworks utilized (disulfide-bridged di-α-helical peptides, helix-loop-helix peptide, and a disulfide-bridged pair of helix-loop-helix peptides) demonstrating the gross features of these topologically related four helix bundles. Sequence alignment of the peptides studied is given in single letter code.

where P is the molar concentration of total monomeric protein, $K_{unf} = \exp(-\Delta G_{unf}/RT)$ and $\Delta G_{unf} = \Delta G^{H_2O} + m[\text{Gdn·HCl}]$, ΔG^{H_2O} is the free energy of the transition in the absence of denaturant, m is the cosolvation term which is a measure of the cooperativity of the transition, and [denaturant] is the concentration of denaturant (M).

The guanidine denaturation curve of (α-*l*-α-SS-α-*l*-α) was fit to the following equation for a monomer folded to monomer unfolded equilibrium (*37*):

$$\text{fraction folded} = \frac{\exp(\Delta G^{H_2O} - m[\text{Gdn·HCl}])}{1 + \exp(\Delta G^{H_2O} - m[\text{Gdn·HCl}])}$$

Infrared Spectroscopy. Fourier transform infrared spectra were recorded on a Bruker IFS 66 FT-IR spectrometer equipped with a Globar source, a KBr beam splitter, and a mercury−cadmium−telluride detector. A sample holder of 0.05 mm path length with CaF_2 windows was used for IR measurements.

Design Strategies for Conversion of (α-SS-α)$_2$ into (α-l-α)$_2$ and (α-l-α-SS-α-l-α). Two peptides were designed to convert the prototype four helix bundle heme protein maquette, [H10H24]$_2$ or (α-SS-α)$_2$, comprising two disulfide-linked α-helices, α_2, into a single molecule four helix bundle, α_4. The design of the prototype (α-SS-α)$_2$ peptide, α = {*Ac*-CGGGELWKL·HEELLKK·FEELLKL·HEERLKK·L-*CO-NH$_2$*}(Figure 1), is an amalgamation of the features of the designed [α_2]$_2$ (*38*) and the natural cytochrome *bc*$_1$ complex (*39*−*41*). Each of the 27 residue helices contains minor variations of four minimalist designed coiled-coil (*42*,*43*) heptad repeats of (Leu$_a$-Glu$_b$-Glu$_c$-Leu$_d$-Leu$_e$-Lys$_f$-Lys$_g$)$_4$ with an N-terminal Cys-(Gly)$_3$ linker denoted as (-SS-). Heme binding histidines were placed in four heptad *a* positions in the (α-SS-α) monomer (H10, H10′, H24, and H24′) spaced 14 amino acids apart (two heptads) as observed in the cytochrome *bc*$_1$ complex (His97 and His111; *Rhodobacter capsulatus* numbering). Two additional residues were incorporated on the basis of the cytochrome *bc*$_1$ complex sequence (*39*); the phenylalanine at 17 in the central heptad *a* position (analogous to Phe104) separates the two heme binding sites, and the arginine located at heptad *d* position 27 (*bc*$_1$ counterpart, Arg94) modulates the redox potential of the heme bound at the H24,H24′ site. The properties of (α-SS-α)$_2$ are consistent with a well-folded four α-helix bundle with a non-native hydrophobic core; however, a double helix modification, [H10H24-L6I,L13F]$_2$ or (α′-SS-α′)$_2$ (sequence in Figure 1), is capable of transforming this *apo* peptide into a uniquely structured hydrophobic core amenable for structural elucidation by NMR methods (*15*).

Two helix-loop-helix peptides, (α-*l*-α)$_2$ and (α′-*l*-α′)$_2$, were designed to conserve the general features of (α-SS-α)$_2$ and (α′-SS-α′)$_2$ while removing the N-terminal disulfide. In each case, two helical regions of 27 amino acids were joined by a rudimentary turn of eight glycines chosen for their ability to adopt a wide range of backbone dihedral angles. The length of the loop was kept consistent with the disulfide-bridged loop region of the (α-SS-α) and (α′-SS-α′) monomers to minimize any adverse effects due to the loop character in this redesign. The helices contain analogous heme binding histidines in heptad *a* positions (8, 22, 41, and 54), the central phenylalanine (15) and the pair of arginines (5 and 58), maintained to test the modulation of the potential of the H8,H54 heme binding site by this charge. Thus, the H22,H41 and H8,H54 heme binding sites of (α-*l*-α)$_2$ and (α′-*l*-α′)$_2$ correspond to the previous H10,10′ and H24,H24′ sites in (α-SS-α)$_2$ and (α′-SS-α′)$_2$, respectively. Addition-

ally, in $(\alpha\text{-}/\text{-}\alpha)_2$ a single tryptophan was located at an *e* position toward the end of the N-terminal helix, position 26, as a convenient spectroscopic marker while in $(\alpha'\text{-}/\text{-}\alpha')_2$ the pair of tryptophans were retained from $(\alpha'\text{-SS-}\alpha')_2$. The resulting helix-loop-helix monomers contain hydrophobic cores analogous to those of $(\alpha\text{-SS-}\alpha)_2$ and $(\alpha'\text{-SS-}\alpha')_2$, but the helix macropole direction and side chain packing partners have been altered due to monomer helix reorientation from parallel to antiparallel.

Conversion of the dimeric α_2 architecture of $(\alpha\text{-SS-}\alpha)_2$ and $(\alpha\text{-}/\text{-}\alpha)_2$ into a single α_4 molecule utilized a disulfide. The single molecule four helix bundle was designed by appending a single Cys residue to the N-terminus (heptad *b* position) of the $(\alpha\text{-}/\text{-}\alpha)$ monomer with subsequent oxidation to form the symmetric disulfide. The resulting 126 residue disulfide-bridged monomeric four helix bundle, $(\alpha\text{-}/\text{-}\alpha\text{-SS-}\alpha\text{-}/\text{-}\alpha)$, $\alpha\text{-}/\text{-}\alpha$ = {*Ac*-CL·KKLREEH·LKLLEEF·KKLLEEH·LKWLEGGGGGGGELLKL·HEELLKK·FEELLKL·HEERLKK·L-*CONH*$_2$}, retains the design features of $(\alpha\text{-}/\text{-}\alpha)_2$ with the incorporation of a very short third loop region. The placement of the histidines in heptad *a* positions (9, 23, 42, and 55), the central phenylalanine (16), and the pair of arginines (6 and 59) in $(\alpha\text{-}/\text{-}\alpha\text{-SS-}\alpha\text{-}/\text{-}\alpha)$ is identical to those of $(\alpha\text{-}/\text{-}\alpha)_2$; however, the addition of an N-terminal residue increases their numerical designation. The disulfide imposes a parallel orientation of the helix dipoles in $(\alpha\text{-}/\text{-}\alpha\text{-SS-}\alpha\text{-}/\text{-}\alpha)$, lowering both the translational entropy as well as the number of topological isomers.

RESULTS

Gel Permeation Chromatography. Both the *apo* and *holo* peptides self-assemble in solution to clearly form four helix bundles, as evaluated using gel permeation chromatography with a column standardized with globular proteins. The helix-loop-helix peptides, $(\alpha\text{-}/\text{-}\alpha)$ and $(\alpha'\text{-}/\text{-}\alpha')$, elute (10 mM KP_i, 100 mM KCl, pH 8) with apparent molecular masses of 19.2 and 19.4 kDa (14.6 and 15.0 kDa calculated for the four helix bundles, respectively) consistent with dimerization to form $(\alpha\text{-}/\text{-}\alpha)_2$ and $(\alpha'\text{-}/\text{-}\alpha')_2$. This value is also consistent with the single-molecule four helix bundle, $(\alpha\text{-}/\text{-}\alpha\text{-SS-}\alpha\text{-}/\text{-}\alpha)$, which elutes with an apparent molecular mass of 18.9 kDa (14.9 expected). Moreover, both peptides coelute with $(\alpha\text{-SS-}\alpha)_2$ (apparent molecular mass of 20.1 kDa, 15.1 predicted), previously established to be a four helix bundle by equilibrium sedimentation (*9*) indicating that these related proteins have relatively similar hydrodynamic radii as anticipated. The optical spectra of the *holo* peptides were identical prior to and after elution.

Circular Dichroism of the Apo Peptides. Figure 2 shows the far-UV CD spectra of $(\alpha\text{-SS-}\alpha)_2$, $(\alpha'\text{-SS-}\alpha')_2$, $(\alpha\text{-}/\text{-}\alpha)_2$, $(\alpha'\text{-}/\text{-}\alpha')_2$, and $(\alpha\text{-}/\text{-}\alpha\text{-SS-}\alpha\text{-}/\text{-}\alpha)$ in aqueous buffer. The spectra show minima at 208 and 222 nm, typical of highly α-helical peptides with >80% helical content. The observed $\Theta_{222}/\Theta_{208}$ ratios for $(\alpha\text{-SS-}\alpha)_2$, $(\alpha'\text{-SS-}\alpha')_2$, $(\alpha\text{-}/\text{-}\alpha)_2$, and $(\alpha'\text{-}/\text{-}\alpha')_2$ are all ≥1.0, which is considered diagnostic of coiled coil supersecondary structure (*43*). However, in contrast, the $\Theta_{222}/\Theta_{208}$ ratio for the single-molecule four helix bundle, $(\alpha\text{-}/\text{-}\alpha\text{-SS-}\alpha\text{-}/\text{-}\alpha)$, is significantly lower than 1.0 indicating that the coiled-coil supersecondary structure may be affected by the introduction of the short loop region.

Guanidine Hydrochloride Denaturation. Figure 3 shows the quantitative disruption of both the secondary and tertiary structure of each peptide was accomplished with the chaotropic agent guanidine hydrochloride and observed by CD spectropolarimetry measuring the loss of Θ_{222} ($n \rightarrow \pi^*$ minimum of α-helical systems) at 50 °C, the temperature at which $-\Delta G^{H_2O}$ is maximal for $(\alpha'\text{-SS-}\alpha')_2$. Table 1 summarizes these results which indicate that the reorientation of the helix dipoles and subsequent repacking of the hydrophobic core of $(\alpha\text{-}/\text{-}\alpha)_2$ results in a minor stabilization ($-\Delta\Delta G^{H_2O} \approx +1$ kcal/mol) of the four helix bundle relative to the prototype $(\alpha\text{-SS-}\alpha)_2$. In stark contrast, the data indicate that the reorientation of the helix dipoles and subsequent repacking of the hydrophobic core of $(\alpha'\text{-}/\text{-}\alpha')_2$ results in a significant destabilization ($-\Delta\Delta G^{H_2O} = -6.4$ kcal/mol) of the four helix bundle relative to the uniquely structured $(\alpha'\text{-SS-}\alpha')_2$. The restriction of $(\alpha\text{-}/\text{-}\alpha)_2$ to a monomeric protein, $(\alpha\text{-}/\text{-}\alpha\text{-SS-}\alpha\text{-}/\text{-}\alpha)$, results in increased resistance to chemical denaturation.

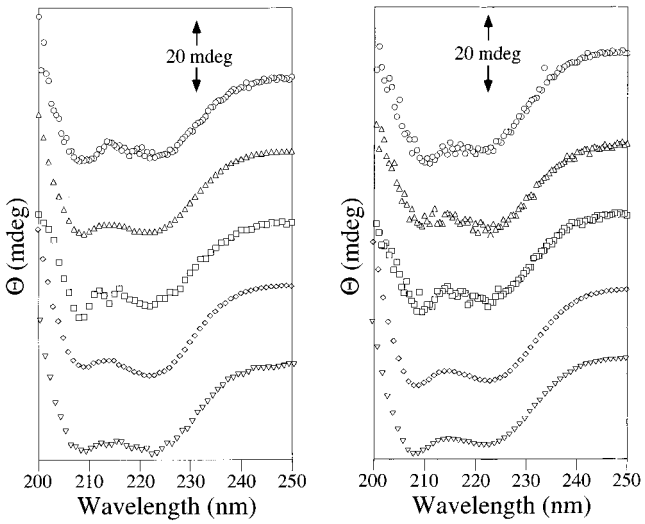

FIGURE 2: Circular dichroism spectra in the UV of 4.75 μM four helix bundle of $(\alpha\text{-SS-}\alpha)_2$ (○), $(\alpha\text{-}/\text{-}\alpha)_2$ (Δ), $(\alpha\text{-}/\text{-}\alpha\text{-SS-}\alpha\text{-}/\text{-}\alpha)$ (□), $(\alpha'\text{-SS-}\alpha')_2$ (◇), and $(\alpha'\text{-}/\text{-}\alpha')_2$, (▽) in the absence (left panel) and the presence of bound heme (right panel). All spectra recorded at 50 °C in 10 mM potassium phosphate, 100 mM KCl, pH 8.5 buffer.

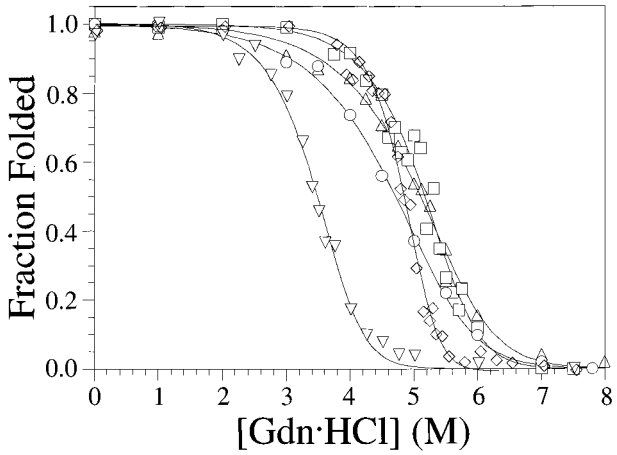

FIGURE 3: Protein denaturation curves of $(\alpha\text{-SS-}\alpha)_2$, (○); $(\alpha\text{-}/\text{-}\alpha)_2$, (Δ); $(\alpha\text{-}/\text{-}\alpha\text{-SS-}\alpha\text{-}/\text{-}\alpha)$, (□); $(\alpha'\text{-SS-}\alpha')_2$, (◇); and $(\alpha'\text{-}/\text{-}\alpha')_2$, (▽) monitored by circular dichroism spectropolarimetery. Spectra were recorded at 50 °C in 10 mM potassium phosphate, 100 mM KCl, pH 8.0 buffer. Peptide concentrations were 3−10 μM as determined spectrophotometrically using Trp (ϵ_{280} = 5600 M^{-1} cm^{-1}). The parameters used to fit each experimental curve are given in the text.

Table 1: Peptide Characterization

peptide	molecular mass: monomer mass	molecular mass: gel permeation	molar ellipticity (222 nm) (deg cm^{-2} dmol^{-1})	% α-helix	[Gdn·HCl]$_{1/2}$ (M)	$-\Delta G^{H_2O}$ (kcal mol^{-1})	m (kcal mol^{-1} M^{-1})
(α-SS-α)$_2$	7575	20 100	25 800	80.5	4.7	14.4	1.4
(α′-SS-α′)$_2$	7643	19 000	27 500	85.9	4.8	23.0	3.2
(α-*l*-α)$_2$	7353	19 200	27 200	85.0	5.1	15.3	1.5
(α′-*l*-α′)$_2$	7490	19 400	23 700	74.0	3.5	16.6	2.5
(α-*l*-α-SS-α-*l*-α)	14910	18 900	25 700	80.3	5.2	11.2	2.1

Table 2: Heme Spectroscopic Properties of *holo*-(α-*l*-α)$_2$

compound	Soret maximum	α/β bands	vis-CD minima
Fe(III)	411 (1.24×10^5 M^{-1} cm^{-1})	530 (1.28×10^4 M^{-1} cm^{-1}) 560 (1.11×10^4 M^{-1} cm^{-1})	412 (3.1×10^4 deg cm^2 dmol^{-1})
Fe(III)(CN)	414 (9.60×10^4 M^{-1} cm^{-1})	536 (1.09×10^4 M^{-1} cm^{-1})	414 (1.8×10^4 deg cm^2 dmol^{-1})
Fe(II)	424 (1.63×10^5 M^{-1} cm^{-1})	529 (1.69×10^4 M^{-1} cm^{-1}) 559 (2.96×10^4 M^{-1} cm^{-1})	424 (3.8×10^4 deg cm^2 dmol^{-1})
Fe(II)(CN)	428 (1.13×10^5 M^{-1} cm^{-1})	532 (1.86×10^4 M^{-1} cm^{-1}) 559 (1.81×10^4 M^{-1} cm^{-1})	428 (1.7×10^4 deg cm^2 dmol^{-1})
Fe(II)(CO)	418 (1.55×10^5 M^{-1} cm^{-1})	536 (1.45×10^4 M^{-1} cm^{-1}) 564 (1.38×10^4 M^{-1} cm^{-1})	418 (2.3×10^4 deg cm^2 dmol^{-1})

Heme Incorporation. Figure 4A−C shows that (α-*l*-α-SS-α-*l*-α) binds four hemes by UV−visible spectroscopy; although not shown, results with (α-SS-α)$_2$ (*9*), (α-*l*-α)$_2$, (α′-SS-α′)$_2$ (*15*), and (α′-*l*-α′)$_2$ are essentially the same. The measurements to determine the individual K_d values were performed over a range of concentrations for optimal assessment. Titration of a 2 mM solution of hemin [ferric-(protoporphyrin IX)Cl] in DMSO into aqueous solutions of 133 nM, 4.85 μM, or 52.3 μM peptide (10 mM KP$_i$, 100 mM KCl, pH 8.0) with agitation results in facile incorporation of heme into the peptide, as evidenced by the Soret maximum at 412 nm ($\epsilon = 1.24 \times 10^5$ M^{-1} cm^{-1} heme^{-1}) and poorly resolved α and β bands at 560 and 529 nm, respectively. After addition of each aliquot, equilibration is complete within 5 min. The four independent K_d values for the pair of H8,H55 and H22,H41 sites of (α-*l*-α-SS-α-*l*-α) were determined to be at 15 nM, 135 nM, 3.5 μM, and 22 μM, shown as insets to Figures 4A−C. Similar values are observed for (α-*l*-α)$_2$ and (α′-*l*-α′)$_2$ (not shown) and reported for (α-SS-α)$_2$ (*9*) and (α′-SS-α′)$_2$ (*15*). Upon heme reduction with sodium dithionite, the optical spectrum displayed a Soret maximum at 424 nm ($\epsilon = 1.60 \times 10^5$ M^{-1} cm^{-1} heme^{-1}), a well-resolved β band at 529 nm ($\epsilon = 1.6 \times 10^4$ M^{-1} cm^{-1} heme^{-1}), and an α-band at 559 nm ($\epsilon = 2.8 \times 10^4$ M^{-1} cm^{-1} heme^{-1}), values typical of bis-histidine ligated *b*-type cytochromes (*44*).

Circular Dichroism of the Holo Peptides. Variances in the *apo* secondary structures were examined after addition of the full complement of four hemes. Far-UV CD measurements of *holo*-(α-SS-α)$_2$, *holo*-(α-*l*-α)$_2$, *holo*-(α′-SS-α′)$_2$, *holo*-(α′-*l*-α′)$_2$, and *holo*-(α-*l*-α-SS-α-*l*-α) were performed under identical conditions (Figure 2, right panel), clearly demonstrating that the addition of four bis-histidine coordinated hemes to the parent peptides results in no significant alteration in the secondary structure of the *apo* peptide; moreover, total α-helical content and coiled-coil character were not significantly altered.

Redox Potentiometry. The reduction potentials of the four hemes in each of the three peptides studied were determined by equilibrium redox titrations. Figure 5 shows the number of hemes reduced as assayed by optical spectroscopy as a function of solution potential for each of the peptides studied. The solid lines drawn though the data points are the nonlinear least-squares fits of each data set to four independent $n = 1$ (fixed) Nernst equations. The four hemes in *holo*-(α-*l*-α)$_2$, *holo*-(α′-SS-α′)$_2$, *holo*-(α′-*l*-α′)$_2$, and *holo*-(α-*l*-α-SS-α-*l*-α) have reduction potentials of −110, −190, −235, and −270 mV (±15 mV) vs NHE, values typical of bis-histidine ligated *b*-type cytochromes and similar to those reported for *holo*-(α-SS-α)$_2$ (*9*). The topological differences between these 3 four helix bundles do not have any significant effect on the E_{m8} values.

Reactions with Exogenous Ligands. Evidence for binding of exogenous ligands to *holo*-(α-SS-α)$_2$, *holo*-(α-*l*-α)$_2$, *holo*-(α′-SS-α′)$_2$, *holo*-(α′-*l*-α′)$_2$, and *holo*-(α-*l*-α-SS-α-*l*-α) was obtained by UV−visible and infrared spectroscopies with Figure 6A showing the spectra and Table 2 summarizing the data for *holo*-(α-*l*-α)$_2$. Addition of KCN to solutions of *holo*-ferric-(α-*l*-α)$_2$ produces changes in the visible absorption spectrum consistent with a single cyanide binding to the each iron(III) of the hemes. The Soret maximum of the *holo*-ferric-(α-*l*-α)$_2$ shifts from 411 to 414 nm, and the α, β bands at 560 and 529 nm coalesce to an unresolved peak at 536 nm. Once formed, the *holo*-ferric-cyanide bound-(α-*l*-α)$_2$ can be reduced with sodium dithionite to produce the *holo*-ferrous-cyanide bound-(α-*l*-α)$_2$ complex with a Soret absorbance at 428 nm and α, β bands at 559 and 532 nm.

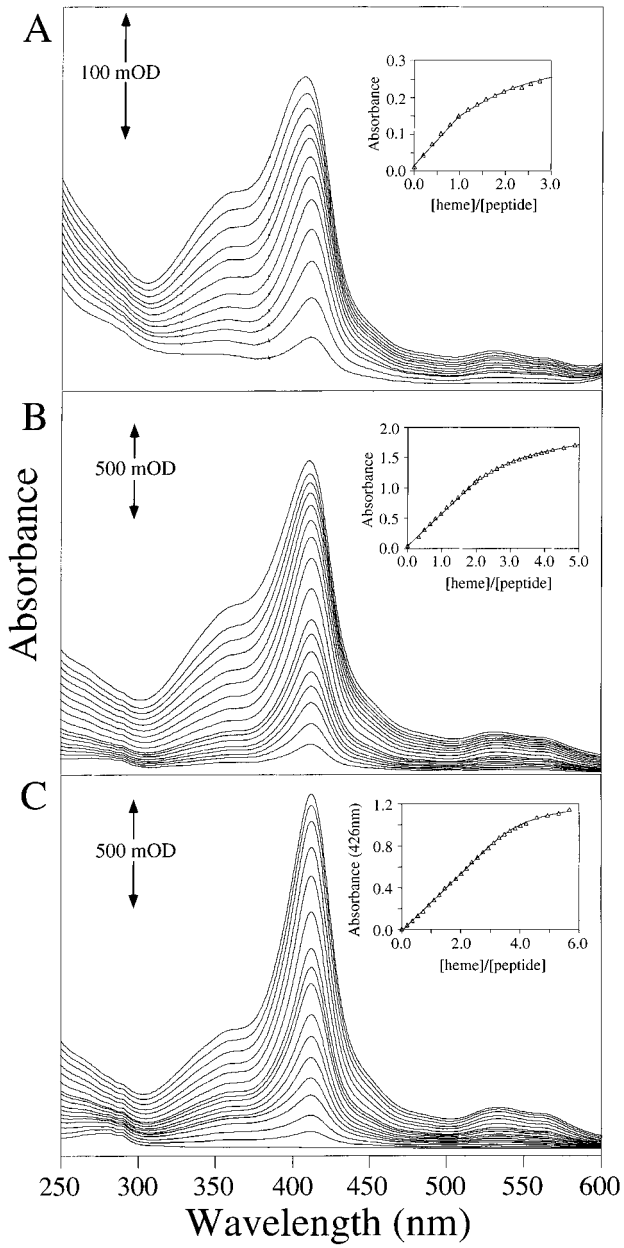

FIGURE 4: (A) Titration of hemin into a 133 nM four helix bundle (α-*l*-α-SS-α-*l*-α) peptide solution recorded in a 10 cm path length cuvette at 25 °C. Spectra shown contain 0.19, 0.39, 0.58, 0.78, 0.98, 1.17, 1.37, 1.56, 1.76, 1.96, 2.15, and 2.35 equiv of added hemin per four helix bundle. (B) Titration of hemin into a 4.86 μM (α-*l*-α-SS-α-*l*-α) solution recorded in a 1 cm path length cuvette. Spectra shown contain 0.33, 0.49, 0.65, 0.81, 0.98, 1.13, 1.30, 1.46, 1.78, 2.11, 2.43, 2.76, 3.08, 3.41, 3.73, 4.06, and 4.55 equiv of added hemin per four helix bundle. (C) Titration of hemin into a 52.3 μM (α-*l*-α-SS-α-*l*-α) peptide solution recorded in a 0.1 cm path length cuvette. Spectra shown contain 0.18, 0.37, 0.55, 0.73, 0.91, 1.09, 1.27, 1.46, 1.64, 1.82, 2.01, 2.37, 2.74, 3.10, 3.47, 3.83, and 4.20 equiv of added hemin per four helix bundle. Insets display the absorbance at 412 nm (for *a*, *b*) or 426 nm (for *c*) vs [heme/four helix bundle] ratio titration curve with fit.

holo-Ferrous-(α-*l*-α)$_2$ also reacts readily with 1 atm of carbon monoxide to quantitatively form the *holo*-ferrous-carbonmonoxy-(α-*l*-α)$_2$ complex. Carbon monoxide causes the Soret of the reduced hemopeptide at 424 nm to bathochromically shift to 418 nm and the intense α, β bands at 559 and 529 nm to redshift to 564 and 536 nm. Figure 6B shows the Soret region CD spectra of each of these exogenous ligand adducts which have negative Cotton effects

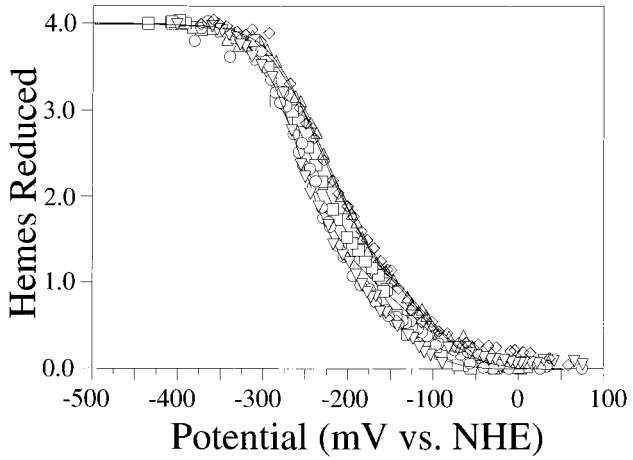

FIGURE 5: Redox titration curves of *holo*-(α-SS-α)$_2$ (○), *holo*-(α-*l*-α)$_2$ (△), *holo*-(α-*l*-α-SS-α-*l*-α) (□), *holo*-(α′-SS-α′)$_2$ (◇), and *holo*-(α′-*l*-α′)$_2$ (▽) monitored by optical spectroscopy at 25 °C. The number of hemes reduced was determined by the change in absorbance at 559 nm (α-band maximum) relative to baseline absorbance (760 nm) normalized to four hemes for the entire titration. Each experimental curve was fit to four independent Nernst equations ($n = 1$ fixed).

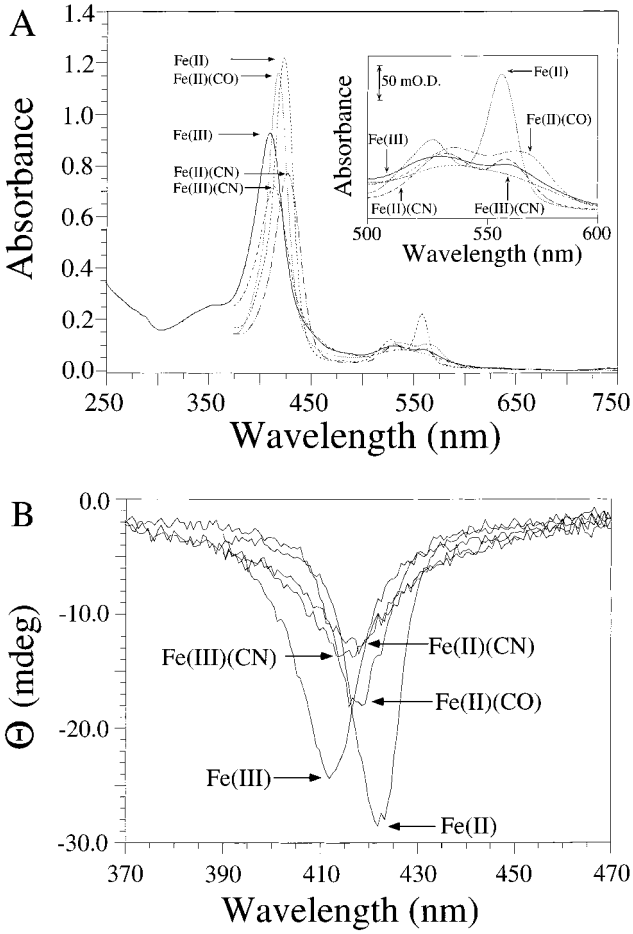

FIGURE 6: Visible (A) optical and (B) CD spectra of *holo*-(α-*l*-α)$_2$ (7.5 μM four helix bundle, 10 mM potassium phosphate, 100 mM KCl, pH 8.0 buffer, at 25 °C) demonstrating binding of exogenous ligands.

at the identical position of the absorbance maximum, illustrating that the heme−exogenous ligand complexes remain in contact with the chiral environment of the peptide. The binding of carbon monoxide to *holo*-ferrous-(α-*l*-α)$_2$ was

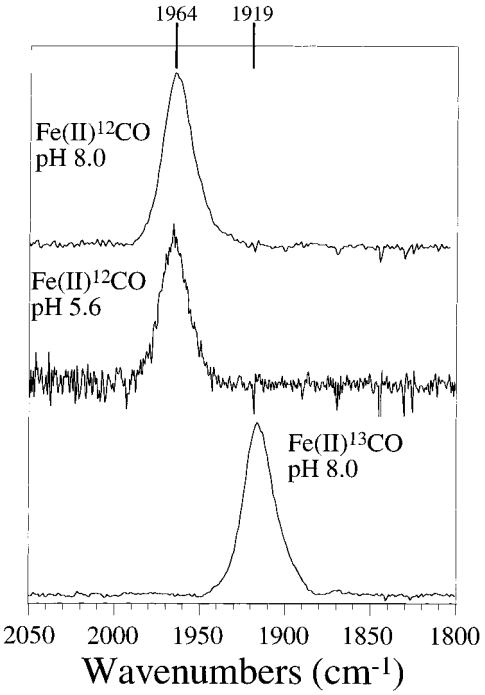

FIGURE 7: Normalized IR absorption spectra of CO bound to *holo*-ferrous-(α-*l*-α)$_2$ recorded at 25 °C. (Top) 200 mM peptide sample at pH 8.0; (middle) 75 mM peptide sample at pH 5.6; and (bottom) ^{13}CO bound to a 300 mM peptide sample at pH 8.0.

further investigated using FT-IR spectroscopy, as the position and linewidth of $\nu_{(CO)}$ can be used as a probe of the protein environment. Figure 7 shows the CO stretching frequency of natural abundance CO bound to the heme at 1964 cm^{-1} at pH 8.0 and pH 5.6, respectively, a position similar to that observed in the carbonmonoxy derivative of a myoglobin mutant, H64L (*45*−*46*), at pH 6.8. The CO stretching frequency of the isotopically labeled ^{13}CO is at 1919 cm^{-1}, consistent with the change in reduced mass of the oscillator. The results obtained with these *holo* peptides clearly shows there is no significant effect on the qualitative reactivity with exogenous ligands regardless of the helix dipole orientation and side chain packing.

DISCUSSION

A pair of four helix bundles, (α-*l*-α)$_2$ and (α-*l*-α-SS-α-*l*-α), related to our prototype heme−protein maquette, (α-SS-α)$_2$ or [H10H24]$_2$, have been utilized to investigate architectural extensions of our designed heme maquette four helix bundle scaffold. These included loop character, helix macropole direction, side chain reorientation from helix repositioning to create new packing partners, and degree of freedom of linkage, i.e., (α$_2$)$_2$ vs α$_4$. Regardless of type of alteration of the topology of the prototype (α-SS-α)$_2$ peptide (helix dipole and side chain reorientation, conformational specificity of the *apo* peptide, dimeric or monomeric four helix bundle), conservation of the relative placement of the histidine, phenylalanine, and arginine residues results in spectroscopic and electrochemical properties for *holo*-(α-SS-α)$_2$, *holo*-(α-*l*-α)$_2$, *holo*-(α′-SS-α′)$_2$, *holo*-(α′-*l*-α′)$_2$ and *holo*-(α-*l*-α-SS-α-*l*-α) which are nearly identical.

The global stability of these peptides is important both for evaluating of the protein design and for judging the effects of helix and side chain reorientation on cofactor incorporation. The stabilities of (α-SS-α)$_2$ and (α-*l*-α)$_2$ are comparable, indicating that the topological rearrangement of the side chains and the requisite creation of new packing partners within the hydrophobic cores of these peptides which possess poorly ordered, conformationally nonspecific (non-native) hydrophobic cores has resulted in only minor perturbation of the global stability in these designed proteins. However, the analogous conversion of a uniquely structured and highly stable four α-helix bundle, (α′-SS-α′)$_2$ or [H10H24-L6I,-L13F]$_2$, to a helix-loop-helix monomer, (α′-*l*-α′)$_2$, is deleterious to both the stability ($-\Delta\Delta G^{H_2O} = -6.7$ kcal/mol) and, more importantly, the conformational specificity of the bundle which is lost. Thus, global reorganization of helix dipoles and side chain packing partners can be accommodated in four α-helix bundles with retention of the global fold, but such reorganization is not tolerated with respect to conformational singularity.

Major global destabilization ($-\Delta\Delta G^{H_2O} = -10.4$ kcal/mol) of the (α-*l*-α)$_2$ peptide results from placement of four histidines within the hydrophobic core with respect to a related peptide, [α$_2$]$_2$, having no histidines (alanines at positions 8, 22, 54, with a cysteine in 41) in the hydrophobic core (*23*). The placement of four polar imidazole rings into heptad repeat *a* positions, directed into the center of the hydrophobic core, has a detrimental effect on global stability of (α-*l*-α)$_2$ as anticipated. However, the parent scaffold, [α$_2$]$_2$, is sufficiently intrinsically stable to accommodate this destabilization, required for subsequent heme incorporation, without significant loss of secondary or tertiary structure. Thus, stable yet conformationally nonspecific protein cores are forgiving enough to accommodate the insertion of polar amino acid ligands into the low dielectric hydrophobic core requisite for engineering of multiple metal cofactor binding sites.

The stability of the monomeric (α-*l*-α-SS-α-*l*-α) cannot be directly compared to the related dimeric proteins, (α-*l*-α)$_2$ and (α-SS-α)$_2$, because of the obvious differences in their unfolded states. However, the midpoint of the unfolding transition and the molar cosolvation term are both greater than those of (α-*l*-α)$_2$, indicating that the reduction to a single molecule has made it more resistant to chemical denaturation. This contrasts with earlier work which has indicated that the use of short loop regions in four helix bundles reduces the global stability and promotes higher order aggregation states (*47*). Our use of a disulfide bond without a glycine linker only minimally affected the helical content, relative to (α-*l*-α)$_2$, and resulted in no marked change in aggregation state of the peptide, suggesting the protein scaffold is flexible enough to accommodate this short turn.

The facile incorporation of four hemes, with dissociation constants in the 15 nM to 25 μM range, does not significantly alter the helical content or aggregation state of the four helix bundles studied, reaffirming the pliable nature of this architecture for the fabrication of maquettes. However, incorporation of four heme macrocycles into the conformationally specific hydrophobic core of (α′-*l*-α′)$_2$ results in loss of unique solution structure. The lowest two K_d values (<200 nM) have been assigned to the H10,H10′ sites of (α-SS-α)$_2$ or [H10H24]$_2$ by spectral and K_d value comparison to the two heme binding alanine variant [H10A24]$_2$. Based on the K_d value, the most likely high-affinity heme binding sites of (α-*l*-α)$_2$, (α′-*l*-α′)$_2$, and (α-*l*-α-SS-α-*l*-α) would

appear to be the analogous H22,H41 and H23,H42 sites, respectively. The heme binding affinity of these three peptides is relatively unaffected by the global four helix bundle topology and the local hydrophobic packing partners, suggesting it may be driven by the use of a common and highly stable ligand geometry within these conformationally diverse peptides.

Aside from providing hydrophobic interactions in the *holo* peptides, the heme porphyrin macrocycle also serves as a spectral probe into protein−cofactor interactions. Circular dichroism spectra of the heme macrocycle imply intimate communication with the chiral peptide environment as symmetrically ligated monomeric porphyrins in isotropic solution are CD inactive. These spectra correlate well with those observed for bis-histidine ligated cytochrome b_{555} for which negative Cotton effect CD spectra were observed in both iron oxidation states (*48,49*). The magnitude of the rotational strength from a symmetrically substituted porphyrin is in agreement with the conclusion of Blauer et al. (*50*) that noncovalent heme protein interactions contribute to the optical activity of the protoheme, perhaps by causing deviations from planarity in the heme macrocycle. Thus, the presence of a CD spectrum independent of the character of the axial heme ligation indicates that the macrocycle is localized in a dissymmetric molecular environment, reflective of nativelike protein−cofactor interactions.

The metal center in each of the *holo* peptides offers an intrinsic electrochemical probe into the surrounding protein environment (*51*). The optical spectra of all five peptides studied, oxidized and reduced, bear a strong resemblance to the electron-transfer protein cytochrome b_{560} which contains a bis-histidine ligated heme (*44*). The reduction potential of the four heme iron ions indicates that the protein effectively shields the heme iron ions from solvent. The most positive reduction potential, −100 mV, is 230 mV higher than that observed for Fe(protoporphyrin IX)$(Im)_2$ in aqueous solution (J. Shifman, personal communication), illustrating the significant effect that the protein environment has on the potential of the iron ions. The observed dispersion in reduction potentials has been ascribed to electrostatic interaction between the arginine residues at positions 27,27′ and the hemes at positions 24,24′ in $(\alpha\text{-SS-}\alpha)_2$ as well as adjacent heme−heme interaction within the low dielectric hydrophobic core of the peptide. The nearly identical electrochemical properties for *holo*-$(\alpha\text{-SS-}\alpha)_2$, *holo*-$(\alpha\text{-}l\text{-}\alpha)_2$, and *holo*-(α-*l*-α-SS-α-*l*-α) indicate that the conservation of the relative placement of the histidine and arginine residues in these topologically related four helix bundles ensures modulation of the redox potential of the bound hemes. Additionally, the similar redox potentials for the bound bound of *holo*-$(\alpha'\text{-SS-}\alpha')_2$ and *holo*-$(\alpha'\text{-}l\text{-}\alpha')_2$ with respect to *holo*-$(\alpha\text{-SS-}\alpha)_2$ and *holo*-$(\alpha\text{-}l\text{-}\alpha)_2$ indicates that conservative alterations to the hydrophobic core do not strongly influence the electrochemical properties of the bound hemes.

The metal center provides a site reactive toward exogenous ligands, a requisite step in the function of heme catalases, oxygenases, and oxidases. The demonstrated binding of cyanide to the oxidized and cyanide or carbon monoxide to the reduced hemes in each of these *holo* peptides indicates that one of the histidine ligands on each heme can be readily displaced by these diatomic molecules, a behavior uncommon to natural bis-histidine ligated cytochromes which typically bind exogenous ligands only upon structural perturbation. For example, cytochrome b_5 only binds cyanide to form ferri-bis-cyano-protoporphyrin IX at high pH where the heme is released from the protein (*52*). The peak position of the FT-IR absorption spectra of the bound CO in *holo*-ferrous-carbonmonoxy-$(\alpha\text{-}l\text{-}\alpha)_2$ indicates that it is similar to that of the carbonmonoxy form of the H64L myoglobin mutant; however, the increased spectral line width from the synthetic protein (16 vs 9 cm^{-1}) indicates that the designed peptide may contain multiple conformations of CO bound to the hemes. This result suggests that the heme binding sites in this synthetic protein are more heterogeneous than the natural protein, which is not unexpected due to the non-native hydrophobic core. Additionally, the FT-IR spectrum of *holo*-ferrous-carbonmonoxy-$(\alpha\text{-}l\text{-}\alpha)_2$ does not show the pH dependence between pH 5.6 and 8.0 observed for wild type (carbonmonoxy)myoglobin which has been attributed to the protonation of the distal histidine. Thus, the possible protonation of the freed histidines in *holo*-ferrous-carbonmonoxy-$(\alpha\text{-}l\text{-}\alpha)_2$ was unobservable in $\nu_{(CO)}$. Last, the reduced heme peptides react within seconds with dioxygen in an autoxidation reaction. While we have not investigated the reduced oxygen species produced from this reaction nor the mechanism (inner or outer sphere electron transfer), nevertheless the data indicate the potential for chemical reactivity at the hemes. The homogeneous reactivity of each of these *holo* peptides regardless of helix macropole orientation and side chain packing partners further indicates the heterogeneous conformational fluxionality of these *holo* peptides.

The construction of synthetic and artificial metalloproteins depends strongly on the proper placement of suitable amino acid ligands in a well-defined structure to modulate the properties of the metal. The conformationally fluxional peptides presented herein allow for the generation of defined hydrophobic cores capable of sustaining local electrostatic fields which result in nativelike heme chromophore properties (nativelike spectroscopy, elevated reduction potentials, heme−heme charge interaction, reactivity with exogenous diatomics) illustrating the potential utility of this type of peptides in the study of metalloproteins. However, the lack of response of the heme properties to structural changes as large as rearrangement of the hydrophobic packing partners and helix dipoles illustrates the limitations of these non-native *holo* peptides. Toward the goal of controlling the heme properties within a maquette, we will utilize the forthcoming NMR structure of *apo*-$(\alpha'\text{-SS-}\alpha')_2$ (J. Skalicky and A. J. Wand, personal communication) and an iterative redesign protocol to provide variants of $(\alpha\text{-}l\text{-}\alpha)_2$ and *holo*-(α-*l*-α-SS-α-*l*-α) suitable for NMR solution structural studies. Using uniquely structured *holo* peptides as a basis for redesign, macrocycle−protein hydrophobic interactions within these heme protein maquettes can be optimized in order to compensate for the loss of iron−ligand bond strength interactions in designs with distorted or unsaturated coordination spheres which may be required for achievement of catalytic fitness (the entatic state).

ACKNOWLEDGMENT

Mass spectroscopic analyses were performed by the Protein Chemistry Laboratory of the University of Pennsyl-

vania. The authors thank Aimee Palmitessa for help with FPLC purification of the hemopeptide samples.

REFERENCES

1. Chance, B. (1966) in *Hemes and Heme Proteins* (Chance, B., Estabrook, R. W., and Yonetani, T., Eds.) Academic Press, New York.
2. Antonini, E., and Brunori, M. (1971) *Hemoglobin and Myoglobin in Their Reactions with Ligands*, North-Holland, Amsterdam.
3. Lemberg, R., and, J. (1973) *Cytochromes*, Academic Press, New York.
4. Schonbaum, G. R., and Chance, B. (1972) in *The Enzymes* (Boyer, P. D., Ed.) Vol. 13, pp 363−388, Academic Press, New York.
5. Hayashi, O. (1962) *Oxygenases*, Academic Press, New York.
6. Babcock, G. T., and Wikström, M. (1992) *Nature 356*, 301−309.
7. Zhang, L., and Guarente, L. (1995) *EMBO J. 14*, 313−320.
8. Varadarajan, R., Zewert, T. E., Gray, H. B., and Boxer, S. G. (1989) *Science 243*, 69.
9. Robertson, D. E., Farid, R. S., Moser, C. C., Urbauer, J. L., Mulholland, S. E., Pidikiti, R., Lear, J. D., Wand, A. J., DeGrado, W. F., and Dutton, P. L. (1994) *Nature 368*, 425.
10. Bryson, J. W., Betz, S. F., Lu, H. S., Suich, D. J., Zhou, H. X., O'Neil, K. T., and DeGrado, W. F. (1995) *Science 270*, 935.
11. Raleigh, D. P., Betz, S. F., & DeGrado, W. F. (1995) *J. Am. Chem. Soc. 117*, 7558.
12. Munson, M., Balasubramanian, S., Fleming, K. G., Nagi, A. D., O'Brien, R. O., Sturtevant, J. M., & Regan, L. (1996) *Protein Sci. 5*, 1584.
13. Braisted, A. C., & Wells, J. A. (1996) *Proc. Natl. Acad. Sci. U.S.A. 93*, 5688.
14. Dahiyat, B. I., & Mayo, S. L. (1997) *Proc. Natl. Acad. Sci. U.S.A. 94*, 10172.
15. Gibney, B. R., Rabanal, F., Skalicky, J. J., Wand, A. J., & Dutton, P. L. (1997) *J. Am. Chem. Soc. 119*, 2323.
16. Jiang, X., Bishop, E. J., & Farid, R. S. (1997) *J. Am. Chem. Soc. 119*, 838.
17. Dolphin, G. T., Brive, L., Johansson, G., & Baltzer, L. (1996) *J. Am. Chem. Soc. 118*, 11297.
18. Kamtekar, S., Schiffer, J. M., Xiong, H., Babik, J. M., & Hecht, M. H. (1993) *Science 262*, 1680.
19. Roy, S., Ratnaswamy, G., Bioce, J. A., Fairman, R., McLendon, G., & Hecht, M. H. (1997) *J. Am. Chem. Soc. 119*, 5302−5306.
20. Kamtekar, S., and Hecht, M. H. (1995) *FASEB J. 9*, 1013.
21. Choma, C. T., Lear, J. T., Nelson, M. J., Dutton, P. L., Robertson, D. E., & DeGrado, W. F. (1994) *J. Am. Chem. Soc. 116*, 856.
22. Kalsbeck, W. A., Robertson, D. E., Pandey, R. K., Smith, K. M., Dutton, P. L., & Bocian, D. F. (1996) *Biochemistry 35*, 3429.
23. Rabanal, F., DeGrado, W. F., & Dutton, P. L. (1996) *J. Am. Chem. Soc. 118*, 473.
24. Rabanal, F., DeGrado, W. F., & Dutton, P. L. (1996) *Tetrahedron Lett. 37*, 1347.
25. Gibney, B. R., Johansson, J. S., Rabanal, F., Skalicky, J. J., Wand, A. J., & Dutton, P. L. (1997) *Biochemistry 36*, 2798.
26. Gibney, B. R., Mulholland, S. E., Rabanal, F., & Dutton, P. L. (1996) *Proc. Natl. Acad. Sci. U.S.A. 93*, 15041.
27. Scott, M. P., and Biggins, J. (1997) *Protein Sci. 6*, 340.
28. Coldren, C. D., Hellinga, H. W., & Caradonna, J. P. (1997) *Proc. Natl. Acad. Sci. U.S.A. 94*, 6635.
29. Sow, T.-C., Pedersen, M. V., Christensen, H. E. M., & Ooi, B.-L. (1996) *Biochem. Biophys. Res. Commun. 223*, 360.
30. Sharp, R. E., Rabanal, F., & Dutton, P. L. (1996) in *Flavins and Flavoproteins* (Stephenson, K., Ed.) pp 163−166, University of Calgary Press.
31. Klemba, M., & Regan, L. (1995) *Biochemistry 34*, 10094.
32. Dieckmann, G. R., McRorie, D. K., Tierney, D. L., Utshig, L. M., Singer, C. P., O'Halloran, T. V., Penner-Hahn, J. E., DeGrado, W. F., & Pecoraro, V. L. (1997) *J. Am. Chem. Soc. 119*, 6195−6196.
33. Pinto, A. L., Hellinga, H. W., & Carradonna, J. P. (1997) *Proc. Natl. Acad. Sci. U.S.A., 94*, 5562.
34. Bodanszky, M. (1993) *Peptide Chemistry: A Practical Approach*, 2nd ed., Springer-Verlag, New York.
35. Dutton, P. L. (1978) *Methods Enzymol. 54*, 411.
36. Mok, Y.-K., De Prat Gay, G., Butler, P. J., & Bycroft, M. (1996) *Protein Sci. 8*, 310.
37. Pace, C. N. (1986) *Methods Enzymol. 131*, 266.
38. Ho, S. P., & DeGrado, W. F. (1987) *J. Am. Chem. Soc. 109*, 6751.
39. Xia, D., Yu, C.-A., Kim, H., Xia, J.-Z., Kachurin, A. M., Zhang, L., Yu, L., Deisenhofer, J. (1997) *Science 277*, 60−66.
40. Trumpower, B. L. (1990) *J. Biol. Chem. 265*, 11409.
41. Ding, H., Moser, C. C., Robertson, D. E., Tokito, M. K., Daldal, F., & Dutton, P. L. (1995) *Biochemistry 34*, 15979.
42. Cohen, C., & Parry, D. A. D. (1986) *Trends Biochem. Sci. 11*, 245.
43. Cohen, C., & Parry, D. A. D. (1990) *Proteins: Struct., Funct., Genet. 7*, 1.
44. Yu, L., Xu, J.-X., Haley, P. E., & Yu, C.-A. (1987) *J. Biol. Chem. 262*, 1137.
45. Balasubramanian, S., Lambright, D. G., & Boxer, S. G. (1993) *Proc. Natl. Acad. Sci. U.S.A. 90*, 4718−23.
46. Balasubramanian, S., Lambright, D. G., Simmons, J. H., Gill, S. J., & Boxer, S. G. (1994) *Biochemistry 33*, 8355−60.
47. Predki, P. F., & Regan, L. (1995) *Biochemistry 34*, 9834−9839.
48. Okada, Y., & Okunuki, K. (1970) *J. Biochem. 67*, 487.
49. Okada, Y., & Okunuki, K. (1970) *J. Biochem. 67*, 603.
50. Blauer, G., Sreerama, N., & Woody, R. W. (1993) *Biochemistry 32*, 6674.
51. Vallee, B. L., & Williams, R. J. P. (1968) *Proc. Natl. Acad. Sci. U.S.A. 65*, 498.
52. Labbe-Bois, R. (1972) in *Structure and Function of Oxidation−Reduction Enzymes* (Åkeson, Å., and Ehrenberg, A., Eds.) pp 303−308, Pergamon Press, New York.
53. Baca, M., Scanlan, T. S., Stephenson, R. C., and Wells, J. A. (1997) *Proc. Natl. Acad. Sci. U.S.A. 94*, 10063.

BI971856S